ADVANCED FUNCTIONAL MATERIALS
www.afm-journal.de

Structural and Electronic Properties of Crystalline, Isomerically Pure Anthradithiophene Derivatives

*Rawad K. Hallani, Karl J. Thorley, Yaochuan Mei, Sean R. Parkin, Oana D. Jurchescu, and John E. Anthony**

Anthradithiophene chromophores are found in many current high-performance organic semiconductors, even though these materials are typically synthesized as an inseparable mixture of *syn* and *anti* isomers. Recent syntheses of pure *syn* anthradithiophenes have shown no improvement in performance for the more homogeneous system, but similar studies on the pure *anti* isomer have not been reported. In this work, a simple protocol is described to prepare the pure *anti* isomer of fluorinated, functionalized anthradithiophenes, and perform detailed analysis of the intermolecular interactions in the crystal that yield increased density and closer chromophore contacts. Studies of the charge-transport properties of these pure isomers, compared to the isomeric mixtures, suggest that the benefit of isomer purity is not consistent; in the *syn* case, there was minimal difference between the pure isomer and the mixture, while for the *anti* isomer mobility improved nearly twofold. Analysis of disorder in the crystals suggests a reason for this difference in performance.

1. Introduction

Anthradithiophene (ADTs, **Figure 1**) semiconductors, introduced by Katz and co-workers,[1] have become a common core in both small-molecule and polymeric semiconductor systems.[2] Incorporated into polymer backbones, ADTs have yielded materials with hole mobility extracted from field-effect transistor (FET) devices on the order of 0.1 $cm^2\ V^{-1}\ s^{-1}$.[3] The solubilized small-molecule versions of this chromophore fare significantly better in this application, exhibiting impressive hole mobilities as high as 6 $cm^2\ V^{-1}\ s^{-1}$,[4] and have proven amenable to a vast array of different processing conditions.[5] These impressive charge transport properties are surprising, considering that the majority of devices based on ADTs reported to date have been formed from a material consisting of a mixture of isomers. Typically, isomeric mixtures are expected to offer decreased electronic performance, due to the inhomogeneities in intermolecular order that arise in the crystalline state.[6]

The isomer mixtures (*mix* ADTs) arise due to the nonregiospecific aldol condensation used in the most common synthesis of the ADT chromophore.[7] Even in the case of highly soluble ADT derivatives, separation of the *syn* and *anti* isomers after synthesis has proven impossible. Thus the chemical community has adopted much lengthier synthetic approaches to synthesize each pure isomer directly. Geerts and co-workers were the first to explore pure ADT isomers, developing an elegant synthesis of pure *anti* dihexyl ADT with an overall chemical yield of ≈3% in 2011.[8] Unfortunately, there have been no reports of the device performance/hole transport property measurement for this material. In 2012, the Tykwinski group demonstrated the first synthesis of pure *syn* diF TES ADT, in an overall yield of 9% from commercial starting materials.[9] Single-crystal studies by Jurchescu and co-workers showed no significant difference in charge transport properties between the *mix* and *syn* materials.

More recently, Takimiya and co-workers prepared the parent ADT in isomerically pure *anti* form in six synthetic steps and 43% overall yield,[10] and found that the transistor performance was several times higher than that of the isomeric mixture reported by Katz[1] (although some of this improvement may arise due to improved modern device fabrication protocols). Mamada and co-workers prepared *both* isomeric forms of the parent ADT, in 12% overall yield for *anti* and 7% yield for *syn*.[11] In vacuum-deposited devices, the *anti* isomer showed substantially higher performance than the *syn* isomer; 0.18 $cm^2\ V^{-1}\ s^{-1}$ compared to 0.017 $cm^2\ V^{-1}\ s^{-1}$ for *syn*. Similarly, Takimiya and co-workers also observed an order-of-magnitude difference in hole transport efficiency between alkylated isomerically pure *anti*- and *syn*-naphthodithiophenes, with the *anti* derivative again exhibiting better performance.[12] These results strongly suggest that a detailed understanding of the impact of isomer mixtures in the solution-processable, ethyne-substituted ADTs will not be complete without side-by-side analysis of the *mix*, *syn*, and heretofore-elusive pure *anti* isomers.

R. K. Hallani, Dr. K. J. Thorley, Dr. S. R. Parkin, Prof. J. E. Anthony
Department of Chemistry
University of Kentucky
Lexington, KY 40506-0055, USA
E-mail: anthony@uky.edu
Y. Mei, Prof. O. D. Jurchescu
Department of Physics
Wake Forest University
Winston-Salem, NC 27109, USA

DOI: 10.1002/adfm.201502440

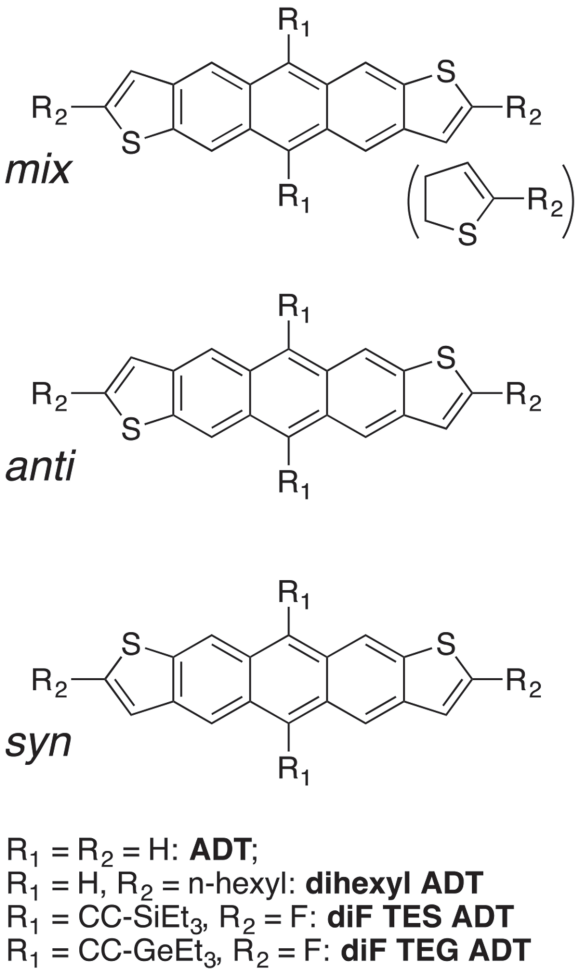

Figure 1. Structures of the anthradithiophene derivatives discussed in this study.

Because the direct synthesis of isomerically pure ADTs is lengthy and typically exhibits low product yield,[13] we were curious whether a chromatographic separation might be possible. While the maximum yield of any particular isomer is 50% by this route (assuming *syn* and *anti* are formed in similar amounts during the regio-random synthesis), the smaller number of higher-yielding synthetic steps in this route allow for scaling of the reactions, and should provide an overall increased throughput in synthesis. Additionally, pure *syn* isomer will also be produced by this method as a byproduct, allowing side-by-side comparison of *anti*, *syn*, and *mix* ADT systems.

2. Results and Discussion

2.1. Synthesis

Recent efforts in the Anthony group toward the synthesis of highly desymmetrized silylethyne ADTs suggested that such molecules do indeed allow the separation of isomers by standard silica-based chromatographic methods, due to the better exposure of the polar sulfur atoms to the chromatographic environment. We thus chose the monosilylated diethynyl anthradithiophenes **1(a–c)** as our synthetic target. The isomeric mixture of this ADT molecule is prepared in two synthetic steps in 41% yield as outlined in **Scheme 1**, and although slightly unstable in concentrated solution, these isomers are easily separated by silica gel column chromatography using an automated system (eluting with hexanes). Crystallographic characterization of these stable molecules did indeed show the separation of the three expected isomers as shown in the scheme (thermal-ellipsoid plots confirming isomer structures are shown in the Supporting Information).

The isolated isomers were then quickly converted to the final semiconductors as shown in Scheme 1. Each isomer of **1** was first fully desilylated, then the desired alkyne cap was installed by stirring the poorly soluble diethynyl ADT in a solution of silyl (or germyl) chloride and the non-nucleophilic base lithium bis(trimethylsilyl)amide. The *anti* isomer in this case was formed in an overall 14% yield from commercially available starting materials. The *syn* isomer was also formed, in overall ≈4% isolated yield.

2.2. Structural Characterization

X-ray crystallographic analysis of *anti* diF TES ADT and *anti* diF TEG ADT showed that both isomers adopted solid-state arrangements nearly identical to those observed from the corresponding isomeric mixtures. However, in both cases there were small decreases in interatomic spacing in structures acquired at the same temperature—and in the case of diF TEG ADT, we observed a small but significant increase in density of the crystal that suggests tighter overall intermolecular interactions.

To determine whether these changes alter the electronic coupling between chromophores in the solid, we performed charge-transfer integral calculations based on the obtained crystal structures. To achieve this, we used the localized monomer approach[14] with Gaussian09,[15] using the B3LYP/6–31G(d) functional and basis set. As a 2D π-stacked material, each ADT chromophore interacts with two symmetry-related pairs of molecules in the solid state. **Figure 2** shows the appropriate stacking partners, consisting of one strongly interacting (dark oval) and one weakly interacting (light oval) ADT molecule. The calculated electronic couplings derived from the crystal structures of both the *anti* and *mix* ADT isomers (as well as the *syn* diF TES ADT)[9] show that in both the TES and TEG case, the electronic coupling is stronger for the *anti* ADT—and in the case of the TEG compound, the difference is substantial. It should be noted that even in the isomerically pure materials, some positional disorder of the thiophene rings exists (as described below); the couplings listed in Figure 2 correspond to those for the crystallographically most common arrangement of molecules.

2.3. Device Studies: Hole Transport Properties

To investigate the impact of isomer purity on device performance and hole transport properties, we fabricated organic thin-film transistors (OTFTs) based on both the isomeric mixture, the *syn* and *anti* isomers of TES and TEG, respectively. To

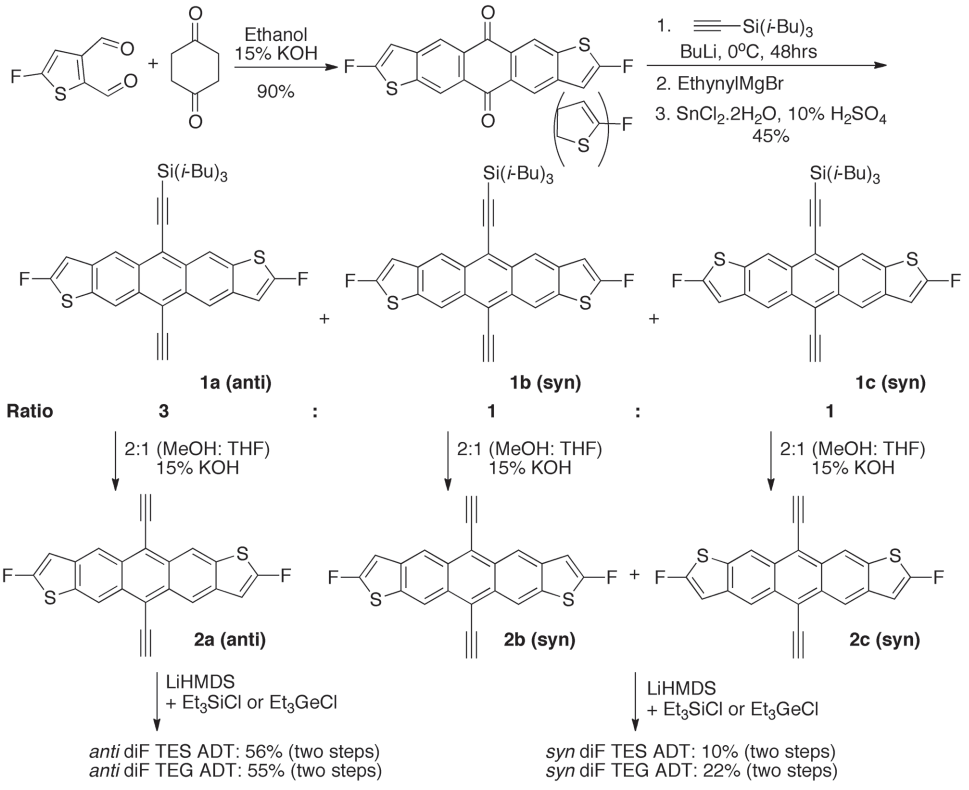

Scheme 1. Synthesis of pure *syn* and *anti* diF ADT isomers by chromatographic separation.

accurately compare device performance across all compounds, all devices investigated here maintained a similar structure (**Figure 3**). Bottom contact, top gate OTFTs were fabricated by spin-coating the organic semiconductor on gold source-drain electrodes chemically modified with pentafluorobenzenethiol (PFBT) to improve injection and film crystallization.[16] An amorphous fluoropolymer gate dielectric known as Cytop (Asahi Glass) was used as the dielectric, with Al top gate electrode. For comparison, the pure *syn* isomer was studied along with the mixture of isomers and the pure *anti* isomer.

The devices were measured in the dark under air, using an Agilent 4155 C semiconductor parameter analyzer. **Figure 4** illustrates typical current–voltage characteristics for representative *mix* diF TES ADT (a), *syn* diF TES ADT (b), *anti* diF TES ADT (c), *mix* diF TEG ADT (d), *syn* diF TEG ADT (e), *anti* diF TES ADT (f) devices. These measurements were taken in the saturation regime of OTFT operation (source–drain voltage $V_{DS} = -40$ V). On the right axis we show the drain current I_D, as a function of source–gate voltage, V_{GS}, and on the left axis the square root of I_D, which was used in mobility calculations. Note that these curves show close to zero threshold voltages, sharp turn-on and a well-defined linear dependence of the square root of I_D with V_{GS}, suggesting that our measurements do not suffer from large contact or trapping effects. Similar current–voltage

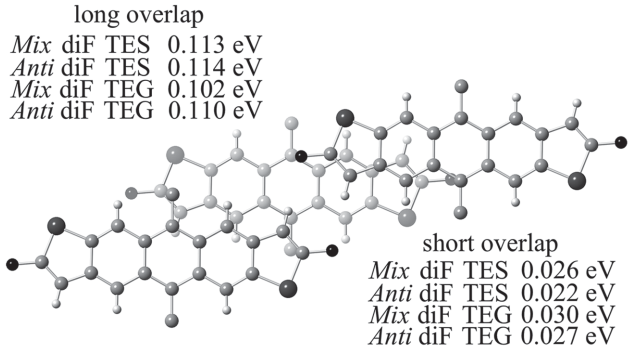

Figure 2. Electronic coupling between π-stacked pairs of *mix* and *anti* diF TES and diF TEG ADTs.

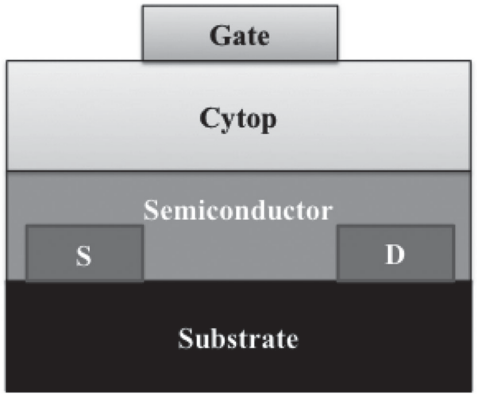

Figure 3. Schematic representation of the bottom-contact, top-gate structure used in this study.

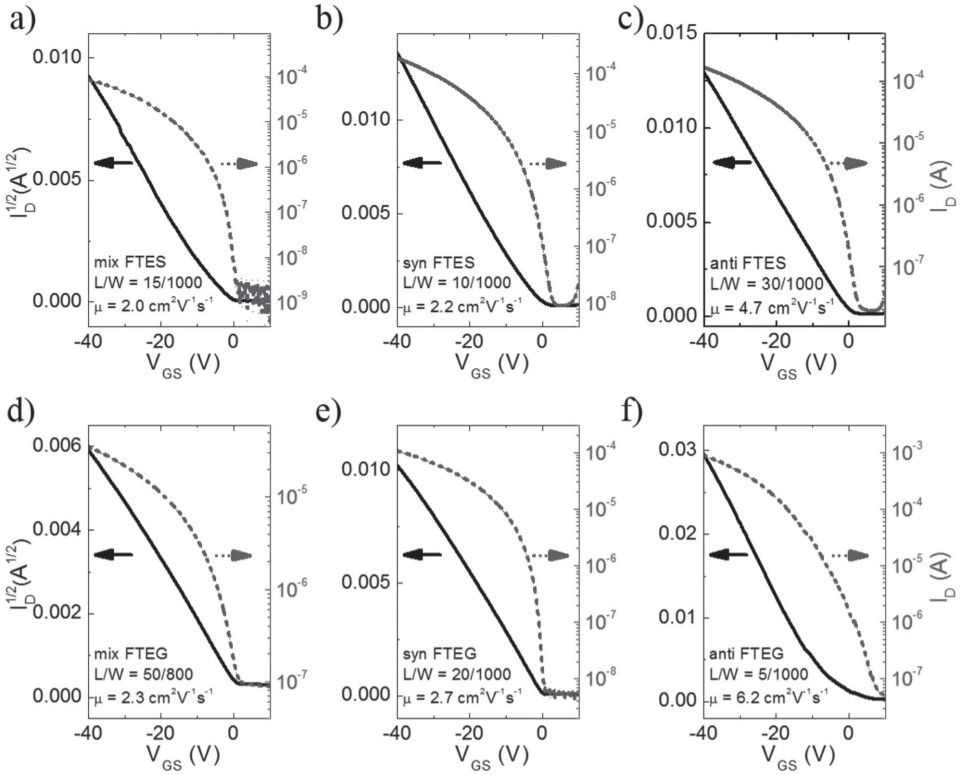

Figure 4. Transfer characteristics of ADT devices: a) *mix* diF TES ADT, b) *syn* diF TES ADT, c) *anti* diF TES ADT, d) *mix* diF TEG ADT, e) *syn* diF TEG ADT, f) *anti* diF TES ADT. The device geometry and mobility are included in the inset.

characteristics for devices of identical geometry are illustrated in Figure S2 of the Supporting Information.

Table 1 shows the average field-effect mobility, μ, of the best six samples studied, as well as the average mobility over all samples studied (>20 for each type of ADT). These mobilities were calculated in the saturation regime of device operation, and the areal capacitance of the dielectric was $C_i = 1.30$ nF cm^{-2}. To minimize the effects of microstructure on the resulting mobilities, we restricted our analysis to devices with channels fully covered with large grains, which in this case consisted of 5 μm ≤ L ≤ 50 μm.[16] We note that the short channel devices (L = 5 μm) exhibit lower mobility values due to significant contributions from the contact resistance. Nevertheless, in all cases the *anti* isomer outperforms both the isomeric mixture and the *syn* isomer, while the *syn* isomer, as suggested by prior studies, exhibited device performance generally on par with that of the mixture of isomers.[8] The performance of the TEG compounds is consistently superior to that of the TES, which is related to the optimized crystalline packing in this compound, as we have shown in an earlier study.[17] While the increase in performance arising from *anti* diF TES ADT is only marginally better than that observed in the isomeric mixture, *anti* diF TEG ADT showed a substantial improvement in performance, yielding spin-cast devices performing at the level of the best single-crystal devices fabricated from *mix* diF TES ADT. This improvement, however, may partially come from the use of Cytop dielectric, which is free of surface-states characteristic to the SiO_2 dielectric used in previous studies on both the TES and TEG compounds.

Table 1. Device performance of *anti*, *mix*, and *syn* ADTs.

Material	Avg. mobility best six samples [cm^2 V^{-1} s^{-1}][a)]	Avg. mobility all samples [cm^2 V^{-1} s^{-1}]
Mix diF TES ADT	2.7 ± 0.7	1.5 ± 0.8
Syn diF TES	3.0 ± 0.4	1.9 ± 0.9
Anti diF TES ADT	4.3 ± 0.8	2.2 ± 1.1
Mix diF TEG ADT	2.4 ± 0.3	1.7 ± 0.6
Syn diF TEG ADT	2.8 ± 0.3	2.2 ± 0.5
Anti diF TEG ADT	6.2 ± 0.4	3.4 ± 1.6

[a)]Dependence of mobility on gate voltage sweep rate is included in the Supporting Information.

2.4. Discussion

The ability to compare crystal structures of the *mix*, *syn*, and *anti* diF ADTs allows us to understand several important issues related to the fine-tuning of crystal packing in these heteroaromatic systems, along with the impact of these subtle changes on charge transport properties. Foremost among these issues is the disordering of the thiophene rings in the *syn*, *anti*, and *mix* cases. For example, in the diF TES ADT series, both isomers and the mix crystallize with

space group P1 with half a molecule in the asymmetric unit. For the pure *syn* molecule, which itself has no inversion center, the presence of an inversion center in the crystal structure at the center of the middle benzene ring forces the disorder fractions for the thiophene rings to be exactly 50:50. In the reported structure, *syn* diF TES ADT[8] the disorder fraction was treated as a variable, which refined to 0.506(2) and 0.494(2). Since any deviation from 0.5 would have indicated contamination by the anti-isomer, it should have been fixed at exactly 0.5. Since the pure *anti* molecule itself has an inversion center, there is no constraint on the thiophene-flip disorder fractions. In the refined model for the *anti* isomer, the fractions refine to 0.891(2) and 0.109(2). For the *mix*, the refined thiophene disorder fractions were intermediate, at 0.688(4) and 0.312(4). For comparison, the *anti* diF TEG ADT fractions refined to 0.944(2):0.056(2) while the mix yielded 0.706(6):0.294(6). These models do not address the question of whether disorder of the ADT core occurs at the individual molecule level or whether it occurs as misoriented clusters of well-ordered molecules. Either way, since the pure *anti* is predominantly (i.e., ≈90% for TES, ≈95% for TEG) in a single orientation, it is clear that the pure *anti* is on the whole substantially more ordered than either the pure *syn* or the *mix*, and that the degree of ordering trends with improvement in charge transport properties.

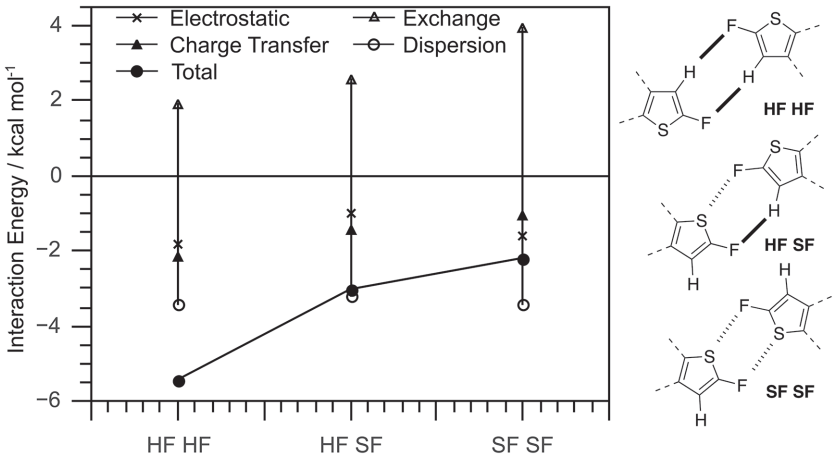

Figure 5. Pairwise interaction energy decomposition analysis for in-plane interactions between the ends of diF ADT dimers interacting through strictly HF coupling (top), a mixture of HF and SF couplings (middle), and exclusive SF couplings (bottom).

Along with issues of improved overall order in the *anti* isomer, the fact that we see increased density for the pure *anti* isomer suggests that there is some form of intermolecular interaction in the *anti* isomer that is weakened or frustrated in the *mix* or *syn* forms. We investigated intermolecular interactions found in the crystal structure by pairwise interaction energy decomposition analysis[18] using the GAMESS software[19] at the MP2 level. This analysis breaks down the van der Waals interaction energies between two molecules into different energy terms to highlight the driving forces stabilizing the interaction. In this case, the in-plane diF ADT dimer was analyzed in three different alignments, with the fluorine atom interacting either with protons or sulfur atoms on the neighboring molecule (**Figure 5**). While the S–F interaction—often cited as an important interaction in many organic semiconductors[20]—is stabilizing, the H–F interaction is three times stronger, and is the major interaction seen in the pure *anti* structure. Assuming the strongest interaction between molecules, the *anti* isomer can form a similar contact with a third molecule, whereas a *syn* isomer must necessarily form a weaker interaction involving sulfur (**Figure 6**). Therefore, the H–F interaction can contribute to the increased order seen in the pure *anti* isomers, as well as decreasing intermolecular distances and giving denser molecular packing, which may explain the stronger electronic coupling and higher charge carrier mobility in the *anti* systems.

Device studies harmonize with our assessments of the crystal structures of the *mix* and *anti* isomers. For the TES compound, the similar values computed for the transfer integral are accompanied by comparable charge transport properties for the devices based on the *anti* TES compared with the mixture ($\mu_{\text{anti-TES}} = 4.3 \pm 0.8$ cm^2 V^{-1} s^{-1} compared with $\mu_{\text{mix-TES}} = 2.7 \pm 0.7$ cm^2 V^{-1} s^{-1}). For the TEG devices, on the other hand, the average mobility for the *anti* isomer is more than double the value of the *mix* sample ($\mu_{\text{anti-TEG}} = 6.2 \pm 0.4$ cm^2 V^{-1} s^{-1} compared with $\mu_{\text{mix-TEG}} = 2.4 \pm 0.3$ cm^2 V^{-1} s^{-1}), in agreement with the larger value obtained for the transfer integral. It is possible that these differences in mobility are even larger, but our measurements on the polycrystalline samples have precluded us from accessing only the strongly interacting π–π stacking direction, which we considered for our calculations. The reduction in mobility for the *mix*-compounds may also originate from the fact that the presence of the disruptive *syn* isomer leads to trapping states for the injected charges. Nevertheless, the small values of the subthreshold slopes recorded in our devices based on *mix*-isomers suggest that this effect, if present, is minor. Another point is that both diF ADTs investigated here form a differential microstructure on the Au and SiO_2 in the presence

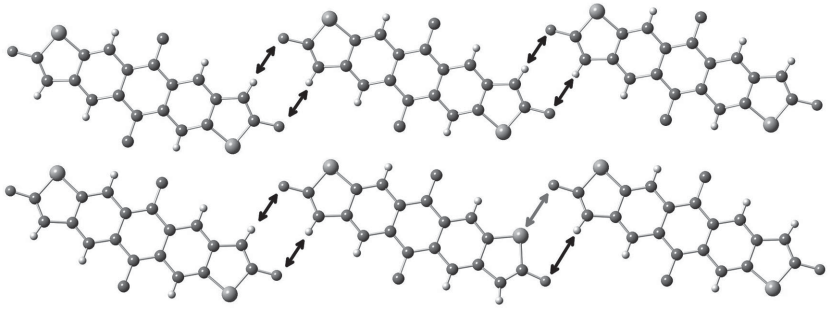

Figure 6. Regular intermolecular F...H interactions (highlighted by black arrows) in the pure *anti* diF ADTs (top) and the loss of one such interaction (gray arrow) required to incorporate the *syn* isomer in *mix* ADTs (bottom).

of PFBT-treated contacts, consisting of large grains of highly oriented molecules bridging narrow contacts and small grains of mixed orientations in the middle of long channels.[13a,b,d] In this work, however, we only focused on the short-channel devices (L < 50 μm), to exclude the microstructure effects from our analysis.

3. Conclusion

We have demonstrated that chromatographic separation of ADT isomers is a convenient approach to the preparation of the pure materials, providing both pure isomers in a single, short synthetic route. Our results from device studies support prior observations that in ethyne-functionalized ADTs, obtaining the pure *syn* isomer offers no substantial benefits to device performance. In this first reported study of the pure *anti* isomers, benefits to device performance rely heavily on the particulars of the system studied. In common with the work by Mamada, the extra steps and decreased yield involved in the preparation of pure *anti* diF TES ADT is not warranted by the small increase in performance of the pure isomer. However, in the case of *anti* diF TEG ADT, the substantial performance enhancement may justify the added effort required to separate the highest-performing compound. More importantly, the ability to study in detail the crystalline motif of each isomer, along with the structure of the corresponding mixture, combined with careful measurement of charge transport properties under identical process conditions, shed light on the precise intermolecular interactions guiding the dense packing of the electronic chromophore. This information will allow refinement of models for crystal packing in this class of heteroacene, assisting development of new design rules for high-performance chromophore design.

4. Experimental Section

ADT Synthesis: Solvents were purchased in bulk from Pharmco-Aaper. Tri-*iso*-butylsilylacetylene was prepared by literature methods.[21] All other chemicals were used as supplied from Sigma-Aldrich. NMR spectra were measured on a Varian (Unity 400 MHz) spectrometer, chemical shifts reported in ppm relative to $CDCl_3$.

Synthesis of 1(a–c): To a nitrogen purged round-bottom flask was added diethyl ether (15 mL), followed by tri-iso-butylsilylacetylene (510 mg, 2.275 mmol). *n*-Butyllithium (1.6 M in hexanes, 1.3 mL, 2.1 mmol) was added dropwise at 0 °C and the mixture was stirred for 1 h while allowing it to reach room temperature. FADT quinone[22] (560 mg, 1.75 mmol) was added to the flask followed by 40 mL of diethyl ether and the reaction was left to stir for 48 h at room temperature. Ethynyl magnesium bromide (0.5 M in THF, 6.8 mL, 3.41 mmol) was added to the reaction mixture, which was stirred for another 2 h. Deoxygenation proceeded by the addition of 5 mL of 10% aqueous H_2SO_4, and stannous chloride dihydrate (2 g, 8.75 mmol) and the mixture was stirred for 30 min. The mixture was then quenched with water and extracted with ethyl acetate, then dried with magnesium sulfate. The solution was then filtered and the solvent was evaporated. The crude product was purified by chromatography on silica using hexanes as the eluent to yield 41% of isomers **1a**, **1b**, and **1c**. The three isomers were recrystallized by slow evaporation from dichloromethane to yield red colored crystals. In general, these poorly stable materials were best kept in dilute solution under nitrogen in the dark.

1a: ^{1}H NMR (400 MHz, $CDCl_3$, δ): 8.81(s,1H), 8.68 (s,1H), 8.67 (s,1H), 8.51 (s, 1H), 6.67 (s, 2H), 4.08 (s, 1H), 2.16 (m, 3H), 1.19 (d, J = 6.94 Hz, 6H), 0.95 (d, J = 6.94 Hz, 6H).^{13}C NMR (100 MHz, $CDCl_3$, δ): 167.28, 167.22, 164.31, 164.25, 163.11, 136.41, 136.33, 136.29, 136.22, 133.75, 133.61, 129.69, 129.56, 129.41, 129.31, 129.27, 120.56, 120.47, 120.19, 120.08, 119.98, 119.73, 117.49, 115.15, 108.45, 103.49, 102.50, 102.40, 102.29, 90.16, 80.60, 67.94, 26.51, 25.38, 25.29.

1b: ^{1}H NMR (400 MHz, $CDCl_3$, δ): 8.69 (s, 2H), 8.63 (s, 1H), 6.67 (s, 2H), 4.04 (s, 1H), 2.16 (m, 3H), 1.19 (d, J = 6.61 Hz, 18H), 0.95 (d, J = 6.93 Hz, 6H). ^{13}C NMR (100 MHz, $CDCl_3$, δ): 167.29, 164.32, 163.12, 136.31, 136.24, 133.67, 129.77, 129.15, 129.12, 120.48, 120.40, 119.76, 114.48, 108.65, 103.61, 102.40, 102.29, 102.26, 102.25, 89.89, 80.51, 67.94, 26.53, 25.33.

1c: ^{1}H NMR (400 MHz, $CDCl_3$, δ): 8.88 (s, 2H), 8.70 (s, 2H), 6.75 (s, 2H), 4.17 (s, 1H), 2.13 (m, 3H), 1.16 (d, J = 6.61 Hz, 18H), 0.92 (d, J = 6.93 Hz, 6H). ^{13}C NMR (100 MHz, $CDCl_3$, δ): 167.29, 164.32, 163.12, 136.31, 136.24, 133.67, 129.77, 129.15, 129.12, 120.39, 120.15, 120.06, 114.48, 108.65, 103.61, 102.40, 102.29, 102.26, 102.25, 89.89, 80.51, 67.94, 26.53, 25.33.

General Procedure for the Synthesis of 2a: in a 100 mL round bottom flask **1a** (290 mg, 0.53 mmol) was dissolved in 5 mL THF and 10 mL methanol. 1 mL of 15% KOH solution was added and the mixture was stirred for 2 h until the solution turned into an orange suspension. The reaction mixture was then filtered and the solid washed with methanol, and dried under high vacuum to yield 160 mg **2a** (80%) as an orange powder. The product was immediately taken to the next step without any further purification.

General Procedure for the Synthesis of Anti diF ADT s: In a flame dried round bottom flask equipped with a stir bar, 160 mg of **2a** was dissolved in 10 mL of dry THF under nitrogen. LiHMDS (1 M in hexane, 0.9 mL, 0.9 mmol) was added dropwise followed by chlorotriethyl silane or chlorotrigermyl silane (1.28 mmol) and the reaction was left to stir for 1 h. After quenching with water and extraction with dichloromethane, the solution was dried ($MgSO_4$) and concentrated under vacuum. The crude product was then purified by silica gel chromatography with hexanes as the eluent, followed by recrystallization from hexanes to yield the pure ADT.

Anti diF TES ADT: ^{1}H NMR (400 MHz, $CDCl_3$, δ): 8.92(s, 2H), 8.84(s, 2H), 6.80(d, J_{FH} = 2.51Hz, 2H), 1.22(t, J = 15.71Hz, 18H), 0.87–0.93 (m, 12H).^{13}C NMR (100 MHz, $CDCl_3$, δ): 167.29, 164.33, 163.10, 136.55, 136.48, 133.86, 130.10, 129.56, 129.52, 121.23, 120.81, 120.56, 120.42, 120.32, 117.46, 107.35, 103.17, 102.68, 102.57, 7.94, 4.80. MS (EI 70 eV) m/z 602 (100%, M^+). Elemental analysis calculated for $C_{32}H_{36}S_2Si$: %C 67.73, %H 6.02, %F 6.30, %S 10.63, Si 9.32. Found: %C 68.32, %H 6.39.

Anti diF TEG ADT: ^{1}H NMR (400 MHz, $CDCl_3$, δ): 8.95(s, 2H), 8.87(s, 2H), 6.79(d, J_{FH} = 2.37 Hz, 2H), 1.29–1.34(m, 18H), 1.11–1.17 (m, 12H).^{13}C NMR (100 MHz, $CDCl_3$, δ): 167.49, 164.52, 163.45, 136.70, 136.63, 133.95, 130.21, 129.89, 129.86, 121.25, 120.80, 120.72, 120.63, 119.98, 117.43, 107.83, 102.94, 102.77, 102.74, 9.73, 6.56. MS (EI 70 eV) m/z 692 (100%, M^+). Elemental analysis calculated for $C_{32}H_{36}S_2Si$: %C 59.01, %H 5.24, %F 5.49, %S 9.27, %Ge 20.99. Found: %C 60.15, %H 5.31.

X-Ray Crystallographic Analysis: X-ray diffraction data were collected at low temperature on either a Nonius kappaCCD (Mo$K\alpha$) or a Bruker X8 Proteum (Cu$K\alpha$) diffractometer. Raw data were integrated, scaled, merged, and corrected for Lorentz-polarization effects using either Denzo-SMN[23] or the APEX2 package.[24] The structures were solved by either SHELXS[25] or SHELXT,[26] and refined with SHELXL.[25] Hydrogen atoms were found in difference maps but subsequently placed at calculated positions and refined using a riding model. Nonhydrogen atoms were refined with anisotropic displacement parameters. Atomic scattering factors were taken from the International Tables for Crystallography.[27] Final models were checked using Platon[28] and by an R-tensor.[29] The CCDC contains the supplementary crystallographic data for the new materials described in this work, including *anti* diF TES ADT (1406651), *anti* diF TEG ADT (1406649), **1a** (1406647), **1b** (1406648), and **1c** (1406650). These data can be obtained free of charge from The Cambridge Crystallographic Data Centre via www.ccdc.cam.ac.uk/data_request/cif.

Calculations: Electronic coupling calculations were performed with Gaussian09,[15] using the B3LYP functional with the 6–31G(d) basis

set. The localized monomer orbital approach was used to account for any site energy differences between interacting molecules. The major molecular alignments observed in the crystal structures were considered. Data for the disordered molecules are available in the Supporting Information. Molecular interaction energy decomposition analysis was performed with GAMESS[16] at the MP2 level using the cc-pVDZ basis set. Atomic coordinates for all input files were taken directly from the crystal structures, including the disordered atoms when considering the minor interactions.

Field-Effect Transistor Fabrication and Characterization: Transistor devices were fabricated on Ti/Au contacts defined by photolithography and deposited by e-beam evaporation over a SiO_2 substrate. The channel lengths L had values between 5 and 100 μm, and widths W of either 800 or 1000 μm. The organic semiconductor was deposited by spin-coating from a 2 wt% solution in room-temperature chlorobenzene, in a nitrogen filled glovebox. Without exposure to air, Cytop dielectric was spun from an undiluted solution on top of the organic semiconductor layer, followed by a curing step at 50 °C in a vacuum oven for 12 h. The devices were completed by Al gate electrodes deposited via thermal evaporation and using a shadow mask.

Supporting Information

Supporting Information is available from the Wiley Online Library or from the author.

Acknowledgements

R.K.H., K.J.T., and J.E.A. thank the NSF (DMR-1035257 and CMMI-1255494) for support of the synthesis of organic semiconductors. Y.M. and O.D.J. thank the NSF (ECCS-1254757 and ECCS-1338012) for supporting their device studies.

Received: June 15, 2015
Revised: August 5, 2015
Published online: November 10, 2015

[1] J. G. Laquindanum, H. E. Katz, A. J. Lovinger, *J. Am. Chem. Soc.* **1998**, *120*, 664.

[2] See, for example, J. Mei, Y. Diao, A. L. Appleton, L. Fang, Z. Bao, *J. Am. Chem. Soc.* **2013**, *135*, 6724, and references therein.

[3] a) Y. Jiang, J. Mei, A. L. Ayzner, M. F. Toney, Z. Bao, *Chem. Commun.* **2012**, *48*, 7286; b) Y. Jiang, T. Okamoto, H. A. Becerril, S. Hong, M. L. Tang, A. C. Mayer, J. E. Parmer, M. D. McGehee, Z. Bao, *Macromolecules* **2010**, *43*, 6361; c) D. Lehnherr, R. Tykwinski, *Aust. J. Chem.* **2011**, *64*, 919.

[4] O. D. Jurchescu, S. Subramanian, R. J. Kline, S. D. Hudson, J. E. Anthony, T. N. Jackson, D. J. Gundlach, *Chem. Mater.* **2008**, *20*, 6733.

[5] For example: a) K. C. Dickey, J. E. Anthony, Y.-L. Loo, *Adv. Mater.* **2006**, *18*, 1721; b) J. Smith, W. Zhang, R. Sougrat, K. Zhao, R. Li, D. Cha, A. Amassian, M. Heeney, I. McCulloch, T. D. Anthopoulos, *Adv. Mater.* **2012**, *24*, 2441; c) A. Pierre, M. Sadeghi, M. M. Payne, A. Facchetti, J. E. Anthony, A. C. Arias, *Adv. Mater.* **2014**, *26*, 5722.

[6] See, for example, a) J.-Y. Balandier, N. Henry, J.-B. Arlin, L. Sanguinet, V. Lemaur, C. Niebel, B. Chattopadhyay, A. R. Kennedy, P. Leriche, P. Blanchard, J. Cornil, Y. H. Geerts, *Org. Lett.* **2013**, *15*, 302; b) T. Okamoto, Z. Bao, *J. Am. Chem. Soc.* **2007**, *129*, 10308; c) T. Okamoto, Y. Jiang, H. A. Becerril, S. Hong, M. L. Senatore, M. L. Tang, M. F. Toney, T. Siegrist, Z. Bao, *J. Mater. Chem.* **2011**, *21*, 7078.

[7] a) P. De la Cruz, N. Martin, F. Miguel, C. Seoane, A. Albert, H. Cano, A. Gonzalez, J. M. Pingarron, *J. Org. Chem.* **1992**, *57*, 6192.

[8] B. Tylleman, C. M. L. Vande Velde, J.-Y. Balandier, S. Stas, S. Sergeyev, Y. H. Geerts, *Org. Lett.* **2011**, *13*, 5208.

[9] D. Lehnherr, A. R. Waterloo, K. P. Goetz, M. M. Payne, F. Hampel, J. E. Anthony, O. D. Jurchescu, R. R. Tykwinski, *Org. Lett.* **2012**, *14*, 3660.

[10] M. Nakano, K. Niimi, E. Miyazaki, I. Osaka, K. Takimiya, *J. Org. Chem.* **2012**, *77*, 8099.

[11] M. Mamada, H. Katagiri, M. Mizukami, K. Honda, T. Minamiki, R. Teraoka, T. Uemura, S. Tokito, *ACS. Appl. Mater. Interfaces* **2013**, *5*, 9670.

[12] S. Shinamura, I. Osaka, E. Miyazaki, A. Nakao, M. Yamagishi, J. Takeya, K. Takimiya, *J. Am. Chem. Soc.* **2011**, *133*, 5024.

[13] M. Nakano, K. Niimi, E. Miyazaki, I. Osaka, K. Takimiya, *J. Org. Chem.* **2012**, *77*, 8099.

[14] E. F. Valeev, V. Coropceanu, D. A. da Silva Filho, S. Salman, J.-L. Brédas, *J. Am. Chem. Soc.* **2006**, *128*, 9882.

[15] Gaussian 09, Revision A.02, M. J. Frisch, G. W. Trucks, H. B. Schlegel, G. E. Scuseria, M. A. Robb, J. R. Cheeseman, G. Scalmani, V. Barone, B. Mennucci, G. A. Petersson, H. Nakatsuji, M. Caricato, X. Li, H. P. Hratchian, A. F. Izmaylov, J. Bloino, G. Zheng, J. L. Sonnenberg, M. Hada, M. Ehara, K. Toyota, R. Fukuda, J. Hasegawa, M. Ishida, T. Nakajima, Y. Honda, O. Kitao, H. Nakai, T. Vreven, J. A. Montgomery Jr., J. E. Peralta, F. Ogliaro, M. Bearpark, J. J. Heyd, E. Brothers, K. N. Kudin, V. N. Staroverov, R. Kobayashi, J. Normand, K. Raghavachari, A. Rendell, J. C. Burant, S. S. Iyengar, J. Tomasi, M. Cossi, N. Rega, J. M. Millam, M. Klene, J. E. Knox, J. B. Cross, V. Bakken, C. Adamo, J. Jaramillo, R. Gomperts, R. E. Stratmann, O. Yazyev, A. J. Austin, R. Cammi, C. Pomelli, J. W. Ochterski, R. L. Martin, K. Morokuma, V. G. Zakrzewski, G. A. Voth, P. Salvador, J. J. Dannenberg, S. Dapprich, A. D. Daniels, Ö. Farkas, J. B. Foresman, J. V. Ortiz, J. Cioslowski, D. J. Fox, Gaussian, Inc., Wallingford, CT, USA **2009**.

[16] a) J. W. Ward, M. A. Loth, R. J. Kline, M. Coll, C. Ocal, J. E. Anthony, O. D. Jurchescu, *J. Mater. Chem.* **2012**, *22*, 19047; b) R. Li, J. W. Ward, D.-M. Smilgies, M. M. Payne, J. E. Anthony, O. D. Jurchescu, A. Amassian, *Adv. Mater.* **2012**, *24*, 5553; c) J. W. Ward, R. Li, A. Obaid, M. M. Payne, D. M. Smilgies, J. E. Anthony, A. Amassian, O. D. Jurchescu, *Adv. Funct. Mater.* **2014**, *24*, 5052; d) C.-H. Kim, H. Hlaing, M. M. Payne, S. R. Parkin, J. E. Anthony, I. Kymissis, *ChemPhysChem* **2015**, *16*, 1251; e) C.-H. Kim, H. Hlaing, J.-A. Hong, J.-H. Kim, Y. Park, M. M. Payne, J. E. Anthony, Y. Bonnassieux, G. Horowitz, I. Kymissis, *Adv. Mater. Interfaces* **2015**, *2*, 1400384.

[17] Y. Mei, M. A. Loth, M. Payne, W. M. Zhang, J. Smith, C. S. Day, S. R. Parkin, M. Heeney, I. McCulloch, T. D. Anthopoulos, J. E. Anthony, O. D. Jurchescu, *Adv. Mater.* **2013**, *25*, 4352.

[18] D. G. Fedorov, K. Kitaura, *J. Comput. Chem.* **2007**, *28*, 222.

[19] M. W. Schmidt, K. K. Baldridge, J. A. Boatz, S. T. Elbert, M. S. Gordon, J. H. Jensen, S. Koseki, N. Matsunaga, K. A. Nguyen, S. Su, T. L. Windus, M. Dupuis, J. A. Montgomery, *J. Comput. Chem.* **1993**, *14*, 1347.

[20] See, for example, a) Y. Wang, S. R. Parkin, J. Gierschner, M. D. Watson, *Org. Lett.* **2008**, *10*, 3307; b) Z. Fei, P. Boufflet, S. Wood, J. Wade, J. Moriarty, E. Gann, E. L. Ratcliff, C. R. McNeill, H. Sirringhaus, J.-S. Kim, M. Heeney, *J. Am. Chem. Soc.* **2015**, *137*, 6866; c) D. J. Crouch, P. J. Skabara, J. E. Lohr, J. J. W. McDouall, M. Heeney, I. McCulloch, D. Sparrowe, M. Shkunov, S. J. Coles, P. N. Horton, M. B. Hursthouse, *Chem. Mater.* **2005**, *17*, 6567.

[21] B. Purushothaman, S. R. Parkin, J. E. Anthony, *Org. Lett.* **2010**, *12*, 2060.

[22] S. Subramanian, S. K. Park, S. R. Parkin, V. Podzorov, T. N. Jackson, J. E. Anthony, *J. Am. Chem. Soc.* **2008**, *130*, 2706.

[23] Z. Otwinowski, W. Minor, *Methods in Enzymology, Macromolecular Crystallography, Part A*, Vol. 276 (Eds: C. W. Carter Jr., R. M. Sweet), Academic Press, New York, NY, USA, **1997**, pp. 307–326.
[24] APEX2, *Programs for Data Collection and Data Reduction*, Bruker-Nonius, Madison, WI, USA **2004**.
[25] G. M. Sheldrick, *Acta Cryst.* **2008**, *A64*, 112.
[26] G. M. Sheldrick, *Acta Cryst.* **2015**, *A71*, 3.
[27] *International Tables for Crystallography, Mathematical, Physical and Chemical Tables*, Vol. C (Ed: A. J. C. Wilson), Kluwer Academic Publishers, Netherlands **1992**.
[28] A. L. Spek, *J. Appl. Cryst.* **2003**, *36*, 7.
[29] S. Parkin, *Acta Cryst.* **2000**, *A56*, 157.